A New Approach to Analytically Solving the Two-Dimensional Poisson's Equation and Its Application in Short-Channel MOSFET Modeling

POLE-SHANG LIN, STUDENT MEMBER, IEEE, AND CHING-YUAN WU, MEMBER, IEEE

Abstract—**An analytical solution for the potential distribution of the two-dimensional Poisson's equation with the Dirichlet boundary conditions has been obtained for the MOSFET device by using Green's function method and a new transformation technique, in which the effects of source and drain junction curvature and depth are properly considered. Based on the calculated potential distribution, the subthreshold current considering the drain-induced barrier lowering effects has been computed by a simple current equation that considers only the diffusion component with an effective length determined by the potential distribution at the SiO_2–Si interface. From the calculated subthreshold current, the threshold voltage of the MOSFET's is determined. It has been verified that the dependences of the calculated threshold voltage and subthreshold current on device channel length, drain, and substrate biases are in good agreement with those computed by whole two-dimensional numerical analysis and experimental data.**

NOMENCLATURE

V_{BI}	The built-in potential between the source and the substrate when the substrate bias is zero.
T_{ox}	The gate oxide thickness.
R_j	The source–drain junction depth.
N_A	The substrate doping concentration.
Y_{d0}	The minimum depletion depth.
R_{SS}/R_{DS}	The radius of the depletion edge of the cylindrical source–drain junction.
L/b	The length/width of the specified rectangular coordinate system.
V_{FB}	The flat-band voltage of the MOSFET.
$\sigma_1(\sigma_2)$	The effective image charge density at the interface.
L^*	The effective length in which the diffusion current dominates.
D_n	The diffusivity of electrons.
W	The effective width of a MOSFET.
Ψ^*	The minimum surface potential.
ϕ	The potential on the boundaries.
ψ	The two-dimensional potential distribution.
V_{BS}	The substrate voltage with respect to the source.
V_{DS}	The drain voltage with respect to the source.
V_{GS}	The gate voltage with respect to the source.

Manuscript received October 22, 1986; revised April 17, 1987. This work was supported by the Electronics Research and Service Organization, the Industrial Technology Research Institute, and the National Science Council, Republic of China, under Grant NSC76-0404-E009-13.

The authors are with the Institute of Electronics, College of Engineering, National Chiao-Tung University, Hsin-Chu, Taiwan, Republic of China.

IEEE Log Number 8715489.

I. INTRODUCTION

FOR A VERY large-scale integration of MOS circuits, the miniaturization of the MOSFET device has been the general trend of technology development. However, due to the scaling of device channel length, the short-channel length effects become extremely important, which have been shown to deteriorate some important device characteristics [1]–[3]. Due to the high sensitivity of the electrical characteristics of short-channel MOSFET's to the process fluctuation, the device design to satisfy a given circuit performance is becoming more difficult, but the problems can be solved by using an accurate device analysis. In the last decade, two-dimensional numerical analysis has been used to investigate many device properties [4], [5]. However, due to excessive computer-time cost and the problem of numerical stability, numerical analysis is not a cost-effective method for circuit simulation and/or statistical modeling in process diagnosis.

Recently, the analytical techniques to characterize short-channel MOSFET's have been obtained by solving the two-dimensional Poisson's equation with approximate boundary conditions. However, the accuracy of the analytical solution for Poisson's equation is strongly dependent on the simplified assumptions used in the derivation. Toyabe *et al.* [6] derived an analytical threshold voltage model, based on a quasi-two-dimensional Poisson's equation; however, they introduced some arbitrary constants to give the best fit in certain ranges of process parameters. Further improvements in this direction were proposed by Wu and Yang [7], in which the effects of source–drain junction depth were included and no empirical constants were required. However, the improved model is only applicable to MOSFET's with uniform substrate doping. In another approach, Ratnakumar and Meindl [8] solved the two-dimensional Poisson's equation with the assumption of infinite junction depth and a constant surface potential along the surface channel. Poole and Kwong [9] improved the model in [8] by replacing the constant surface potential with the normal electric displacement; however, an

0018-9383/87/0900-1947$01.00 © 1987 IEEE

infinite source–drain junction depth was still assumed in order to simplify mathematical derivation. It is well known from the whole two-dimensional numerical analysis that the assumption of infinite source–drain junction depth will overestimate the short-channel effects of MOSFET's. Pfiester *et al.* [10] improved the model in [8] by considering the effects of finite source–drain junction depth; however, the boundary conditions on the source–drain junction were assumed to be the rectangular shape of finite junction depth. It will be discussed later that the short-channel effects are still overestimated by this improved model [10] because the junction curvature is assumed to be too abrupt.

In this paper, we propose a generalized method to solve the electrostatic potential of the two-dimensional Poisson's equation for a MOSFET operated in the subthreshold region. The finite source–drain junction depth is approximated by the cylindrical junction with a radius of R_j. Based on the calculated potential distribution, the subthreshold current and threshold voltage of MOSFET's are investigated. Comparisons between the developed model and the results of whole two-dimensional numerical analysis and experimental data show good agreement for wide ranges of device parameter variations.

II. Analytic Calculations for the Potential Distribution

A. Green's Function

Considering the two-dimensional Poisson's equation in a rectangular coordinate system shown in Fig. 1, the second-order elliptical differential equation for the potential distribution in an n-channel MOS structure can be written as

$$\nabla^2\Psi(x, y) = \begin{cases} 0, & \text{for } 0 < y < T_{ox} \\ -\dfrac{\rho(x, y)}{\epsilon_{si}} = \dfrac{qN_A f(y)}{\epsilon_{si}}, & \text{for } T_{ox} < y < Y_d(x) \end{cases} \tag{1}$$

where N_A is the substrate doping concentration and $f(y)$ is the nonuniform doping function.

The solution of the two-dimensional Poisson's equation in a finite region with the Dirichlet boundary conditions can be obtained by means of Green's function technique. Using Green's theorem in which the Green function on the boundaries is zero for the Dirichlet boundary conditions, the potential distribution $\Psi(x, y)$ is [11]

$$\Psi(x, y) = \iint \frac{\rho(x', y')}{\epsilon} G(x, y; x', y')\, dx'\, dy' - \oint \phi(x', y') \frac{\partial G}{\partial n'}\, ds' \tag{2}$$

where $\nabla^2 G = -\delta(x - x')\,\delta(y - y')$, $\phi(x', y')$ is the potential distribution on the boundaries, n' is the outward direction on the boundaries, and ϵ is the dielectric permittivity that is a constant for a homogeneous system.

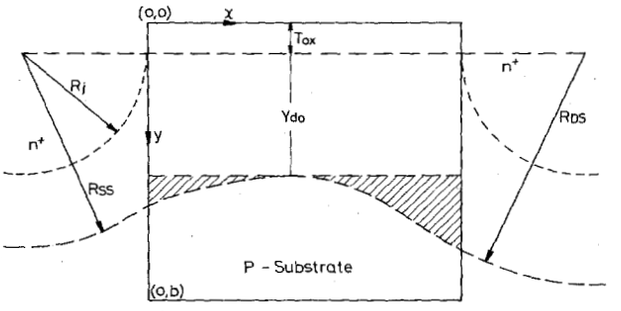

Fig. 1. The schematic cross section of an n-channel transistor in which the rectangular coordinate system is indicated.

The Green function G for a rectangular system shown in Fig. 1 is expressed by

$$\begin{aligned} G(x, y; x', y') &= \frac{2}{L}\sum_{m=1}^{\infty} \sin(k_m x)\sin(k_m x')\, H(y; y'; k_m) \\ &= \frac{2}{b}\sum_{n=1}^{\infty} \sin(k_n y)\sin(k_n y')\, F(x; x'; k_n) \end{aligned} \tag{3}$$

in which $H(y; y'; k_m)$ and $F(x; x'; k_n)$ are

$$H(y; y'; k_m) = \begin{cases} \dfrac{\sinh(k_m y)\sinh k_m(b - y')}{k_m \sinh(k_m b)}, & \text{for } y < y' \\ \dfrac{\sinh(k_m y')\sinh k_m(b - y)}{k_m \sinh(k_m b)}, & \text{for } y' < y \end{cases} \tag{4}$$

$$F(x; x'; k_n) = \begin{cases} \dfrac{\sinh(k_n x)\sinh k_n(L - x')}{k_n \sinh(k_n L)}, & \text{for } x < x' \\ \dfrac{\sinh(k_n x')\sinh k_n(L - x)}{k_n \sinh(k_n L)}, & \text{for } x' < x \end{cases} \tag{5}$$

where $k_m = m\pi/L$, $k_n = n\pi/b$, and m and n are the integers.

Substituting (3) into (2), we obtain

$$\begin{aligned} \Psi_0(x, y) &= \sum_{m=\text{odd}}^{\infty} \sin(k_m x)\frac{\rho_A(m)}{\epsilon}\int_{T_{ox}}^{T_{ox}+Y_{d0}} f(y')\, H(y; y'; k_m)\, dy' \\ &+ \sum_{m=\text{odd}}^{\infty} \sin(k_m x)\cdot\frac{\sinh k_m(b - y)}{\sinh(k_m b)}\cdot\frac{4V'_{GS}}{m\pi} + \sum_{m=\text{odd}}^{\infty} \sin(k_m x)\cdot\frac{\sinh(k_m y)}{\sinh(k_m b)}\cdot\frac{4V_{BS}}{m\pi} \\ &+ \sum_{n=1}^{\infty}\sin(k_n y)\cdot\frac{\sinh k_n(L - x)}{\sinh(k_n L)}\cdot\frac{2}{b}\int_0^b \phi(0, y')\sin(k_n y')\, dy' \\ &+ \sum_{n=1}^{\infty}\sin(k_n y)\frac{\sinh(k_n x)}{\sinh(k_n L)}\cdot\frac{2}{b}\int_0^b \phi(L, y')\sin(k_n y')\, dy' \end{aligned} \tag{6}$$

and

$$\rho_A(m) = \frac{2}{L}\int_0^L (-qN_A)\sin(k_m x')\,dx' \qquad (7)$$

where $\Psi_0(x, y)$ is the potential distribution in a homogeneous system with the same dielectric constant and $V'_{GS} = V_{GS} - V_{FB}$.

In general, the potentials across the source–drain junctions will cause the barrier-lowering effect for short-channel devices, as illustrated in the fourth and the fifth terms on the right side of (6). As the channel length becomes shorter, the perturbations of the potential become serious due to the proximity of the source and drain regions. Note that two approximations have been made in (6). First, the charge contribution to the potential is only evaluated inside the region $T_{ox} \le y \le T_{ox} + Y_{d0}$. This is plausible because the contribution of the other ionized region, i.e., the hatched parts shown in Fig. 1, is proportional to

$$\int_{Y_{d0}+T_{ox}}^{Y_d(x)+T_{ox}} \frac{\sinh(k_m T_{ox})\sinh[k_m(b-y')]}{\sinh(k_m b)}\,dy'. \qquad (8)$$

If $b - y' << b$ is valid in this region, the value of the integral in (8) is negligible. Therefore, the depletion region can be assumed to be independent of the coordinate x for simplicity. Second, it has been assumed in (6) that the dielectrics are uniformly distributed due to the intrinsic property of (2). The different dielectric permittivities for the oxide and the semiconductor always cause difficulty in solving Poisson's equation for a MOSFET. Pfiester *et al.* [10] proposed a transformation method in which the y-coordinate is scaled by a factor of $\epsilon_{si}/\epsilon_{ox}$ throughout the oxide region while assuming an oxide dielectric permittivity of ϵ_{si}. However, as the channel length is reduced, the perturbation of the electric-field lines by the lateral field in the oxide layer as well as in the depletion region will extend over the entire length of the channel [12]. Therefore, the transformation method using the scaled $\epsilon_{si}/\epsilon_{ox}$ becomes less accurate. In the next subsection, a new method called the image charge method will be proposed to solve this problem.

B. Interface Problems for Different Dielectrics

In order to solve the problem resulting from different dielectric permittivities for the oxide and the semiconductor region, a transformation technique is taken and is shown in Fig. 2. From Fig. 2, the effective image charge density $\sigma_1(x)$ is located at the Si–SiO_2 interface and the dielectric permittivity will be assumed to be uniformly distributed with a constant of ϵ_{si} throughout the oxide layer and the silicon region when the observation point is in the silicon region ($T_{ox} \le y \le b$); similarly, the effective image charge density $\sigma_2(x)$ is located at the Si–SiO_2 interface and the dielectric permittivity is a constant of ϵ_{ox} for everywhere when viewed from the oxide region ($0 \le y \le T_{ox}$). According to this transformation technique, the potential $\Psi(x, y)$ must satisfy the continuities of the transverse electric field and normal electric displacement

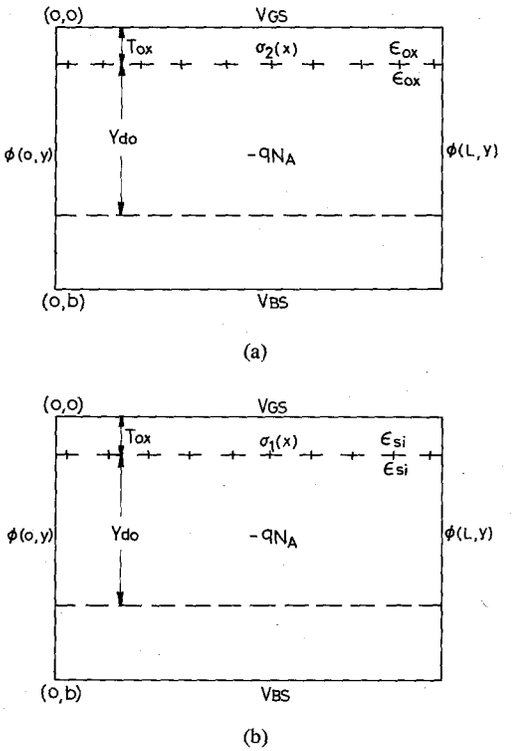

Fig. 2. The transformation technique considering different dielectrics is that the image charge density (σ) is located at the Si–SiO_2 interface and the ionized impurity density ($-qN_A$) is distributed from $y = T_{ox}$ to $T_{ox} + Y_{d0}$ by assuming the same dielectric permittivity (ϵ) for both oxide and semiconductor regions. (a) $\epsilon = \epsilon_{ox}$ and $\sigma = \sigma_2(x)$ when viewed from the oxide region; (b) $\epsilon = \epsilon_{si}$ and $\sigma = \sigma_1(x)$ when viewed from the semiconductor region

at the SiO_2–Si interface, i.e.

$$\frac{\partial}{\partial x}\Psi(x, y)\Big|_{y=T_{ox}^+} - \frac{\partial}{\partial x}\Psi(x, y)\Big|_{y=T_{ox}^-} = 0 \qquad (9a)$$

and

$$-\epsilon_{si}\frac{\partial}{\partial y}\Psi(x, y)\Big|_{y=T_{ox}^+} + \epsilon_{ox}\frac{\partial}{\partial y}\Psi(x, y)\Big|_{y=T_{ox}^-} = 0. \qquad (9b)$$

Note that the fixed charge density at the interface has been lumped into the flat-band voltage V_{FB}. Substituting all the charge densities shown in Fig. 2 into (2), we obtain the potential distribution as follows:

For the oxide region ($0 \le y \le T_{ox}$)

$$\Psi(x, y) = \Psi_0(x, y)\Big|_{\epsilon=\epsilon_{ox}} + \sum_{m=0}^{\infty}\sin(k_m x)\cdot\frac{\sigma_2(m)}{\epsilon_{ox}} \cdot \frac{\sinh k_m(b - T_{ox})\sinh(k_m y)}{k_m \sinh(k_m b)}. \qquad (10)$$

For the silicon region ($T_{ox} \le y \le T_{ox} + Y_{d0}$)

$$\Psi(x, y) = \Psi_0(x, y)\Big|_{\epsilon=\epsilon_{si}} + \sum_{m=0}^{\infty} \sin(k_m x) \cdot \frac{\sigma_1(m)}{\epsilon_{si}} \cdot \frac{\sinh(k_m T_{ox}) \sinh k_m(b - y)}{k_m \sinh(k_m b)} \quad (11)$$

where

$$\sigma_1(m) = \frac{2}{L}\int_0^L \sigma_1(x') \sin(k_m x')\, dx'$$

and

$$\sigma_2(m) = \frac{2}{L}\int_0^L \sigma_2(x') \sin(k_m x')\, dx'.$$

The unknown parameters in (10) and (11) are $\sigma_1(m)$, $\sigma_2(m)$, and Y_{d0}. The values of σ_1 and σ_2 are defined by matching the interface boundary conditions that are derived in the Appendix. The parameter Y_{d0}, as shown in Fig. 1, is determined by $\Psi(X_{min}, T_{ox} + Y_{d0}) = V_{BS}$, in which X_{min} is the position of the minimum potential point along the surface.

Using (10) and (11) the analytic solution for the potential distribution of a MOSFET can be obtained. This general solution is uniquely determined by the given Dirichlet boundary conditions along the rectangular region. It has been stated before that the perturbation of the potential distribution by the source–drain junction is increased as the channel length becomes shorter. Therefore, the boundary values at the source–drain junction and its curvature must be carefully chosen. It is more practical to consider the cylindrical shape than the rectangular shape inherent in the fabrication process; hence, in this paper the finite junction depth is approximated by the cylindrical junction with a radius R_j. It should be noted that this general electrostatic potential distribution can deal with any arbitrary shape and doping profile of the source–drain junction if the specified junction boundaries are given. Similarly, this general solution can be applied to any arbitrary doping profile in the substrate if the nonuniform function $f(y)$ is specified.

C. The Boundary Conditions

In order to demonstrate the applicability of the calculated potential distribution, the doping distribution in the substrate is assumed to be uniform and the boundary conditions for the cylindrical source–drain junction can be expressed as

$$\phi(x, 0) = V'_{GS} \quad (12a)$$

$$\phi(x, b) = V_{BS} \quad (12b)$$

$$\phi(0, y) = \begin{cases} V'_{GS} + \dfrac{V_{BI} - V'_{GS}}{T_{ox}} y, & \text{for } 0 \le y \le T_{ox} \\ V_{BI} + \dfrac{qN_A}{4\epsilon_{si}}(y - T_{ox})^2 - \dfrac{qN_A}{4\epsilon_{si}} R_{SS}^2 \ln\left[1 + \dfrac{(y - T_{ox})^2}{R_j^2}\right], & \\ \quad \text{for } T_{ox} \le y \le T_{ox} + (R_{SS}^2 - R_j^2)^{1/2} & \\ V_{BS}, \quad \text{for } T_{ox} + (R_{SS}^2 - R_j^2)^{1/2} \le y \le b & \end{cases} \quad (12c)$$

$$\phi(L, y) = \begin{cases} V'_{GS} + \dfrac{V_{BI} + V_{DS} - V'_{GS}}{T_{ox}} y, & \text{for } 0 \le y \le T_{ox} \\ V_{BI} + V_{DS} + \dfrac{qN_A}{4\epsilon_{si}}(y - T_{ox})^2 - \dfrac{qN_A}{4\epsilon_{si}} R_{DS}^2 \ln\left[1 + \dfrac{(y - T_{ox})^2}{R_j^2}\right], & \\ \quad \text{for } T_{ox} \le y \le T_{ox} + (R_{DS}^2 - R_j^2)^{1/2} & \\ V_{BS}, \quad \text{for } T_{ox} + (R_{DS}^2 - R_j^2)^{1/2} \le y \le b & \end{cases} \quad (12d)$$

where R_{SS} is determined by

$$V_{BI} - V_{BS} + \frac{qN_A}{4\epsilon_{si}}(R_{SS}^2 - R_j^2) - \frac{qN_A}{4\epsilon_{si}} R_{SS}^2 \ln(R_{SS}/R_j) = 0 \quad (13a)$$

and R_{DS} is determined by

$$V_{BI} + V_{DS} - V_{BS} + \frac{qN_A}{4\epsilon_{si}}(R_{DS}^2 - R_j^2) - \frac{qN_A}{4\epsilon_{si}} R_{DS}^2 \ln(R_{DS}/R_j) = 0. \quad (13b)$$

Note that all of the potential voltages are referred to the substrate with $V_{BS} = 0$ and V_{BS} is negative for the p-type substrate. The above Dirichlet boundary conditions are different from those used by Ratnakumar and Meindl [8] and Toyabe and Asai [6]. From (12), the boundary at $y = L$ is at the neutral region and the potential along this line is equal to V_{BS}. The potential in the oxide along the boundaries, $x = 0$ and $x = L$, is assumed to have the uniform electric field and, therefore, its potential is a linear function of y. The resulting errors due to the above assumption are small because the oxide thickness (T_{ox}) is much less than the box width (b). Therefore, the contribution of these parts of boundaries to the potential distribution is negligible. For $t_{ox} \leq y \leq b$ along $x = 0$ and $x = L$, the potential distributions in the cylindrical junction as shown in (12c) and (12d) are calculated by using a one-dimensional model. Note that we have assumed that the electric field along the rectangular boundary ($T_{ox} \leq y \leq b$) is almost induced by the nearest cylindrical junction and the potential distribution is equal to that of the isolated junction. This approximation therefore is valid before the onset of hard drain-induced punchthrough.

D. Some Results and Discussions

The convergent rate in (11) depends on the magnitude of the effective channel length. It is shown that the shorter the effective channel length, the less number of terms needed in (11) because the value of hyperbolicsine function decays very quickly. If we are only interested in some local behavior (e.g., the potential distribution in the certain portion of the surface channel), the computation time is much less than that of the two-dimensional numerical analysis. Fig. 3 shows the calculated potential distribution along the surface, under the condition that the gate voltage strongly inverts the minimum surface potential point. It is shown that the potential distribution has a minimum value and the minimum point shifts to the source as the channel length is decreased. This fact is consistent with the result calculated by the two-dimensional numerical analysis [6]. Fig. 4 shows that the depletion depth Y_{d0} is increased with decreasing channel length. This effect is due to the divergence of the lateral electric field [12]. Fig. 5 shows the potential distribution along $y = Y_{d0} + T_{ox}$ versus different channel lengths. It is clearly seen that although the ionized impurity concentration outside the minimum depletion depth Y_{d0} has been ignored, the potential along this line ($y = T_{ox} + Y_{d0}$) is not a constant. Therefore, the error produced by our previous assumption that the depletion depth is independent of the coordinate x is negligible. Moreover, the effect of the wider depletion depth on the surface potential is not significant. From (6), the contribution of the ionized impurity concentration to the surface potential distribution is proportional to

$$\int_{T_{ox}}^{T_{ox}+Y_{d0}} \frac{\sinh k_m(b - y')}{\sinh (k_m b)}\, dy' = \int_{T_{ox}}^{T_{ox}+Y_{d0}} \exp(-k_m y')\, dy' \qquad (14)$$

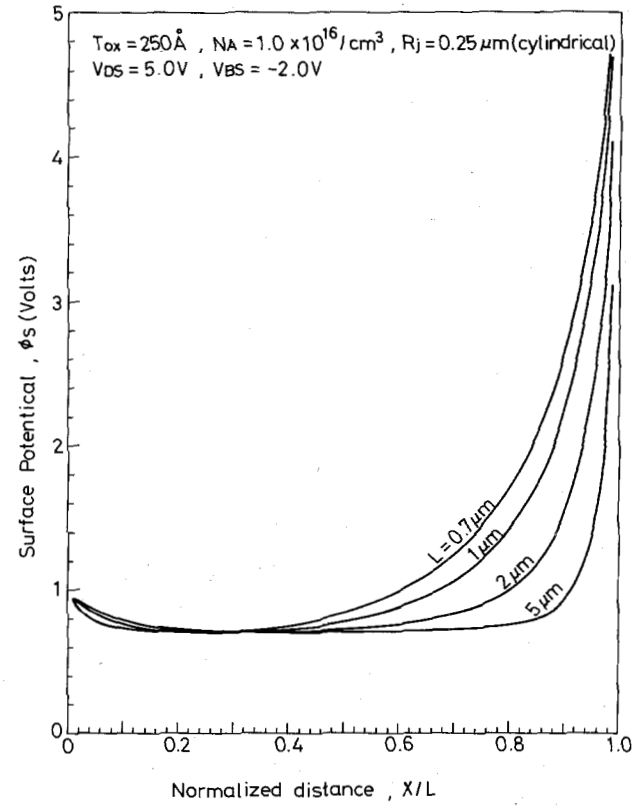

Fig. 3. The calculated band bending along the surface channel ($y = T_{ox}$) when the gate voltage strongy inverts the minimum surface potential point.

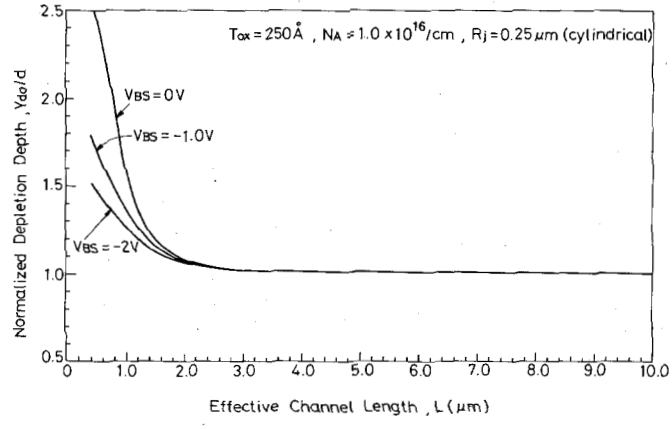

Fig. 4. The calculated minimum depletion depth (Y_{d0}) versus the effective channel length, in which the normalized factor is the depletion depth of long-channel MOSFET's.

in which the exponential function decays very quickly as the channel length is reduced. Although the depletion region of short-channel MOSFET's is wider than that of long-channel devices, the threshold voltage is still decreased for short-channel devices because of the screened impurity effect as illustrated in (14) and the barrier-lowering effect by the potentials across the source–drain junctions. Therefore, the minimum depletion depth (Y_{d0}) can be obtained by the depletion depth calculated by the one-dimensional model when only the surface potential distribution is concerned.

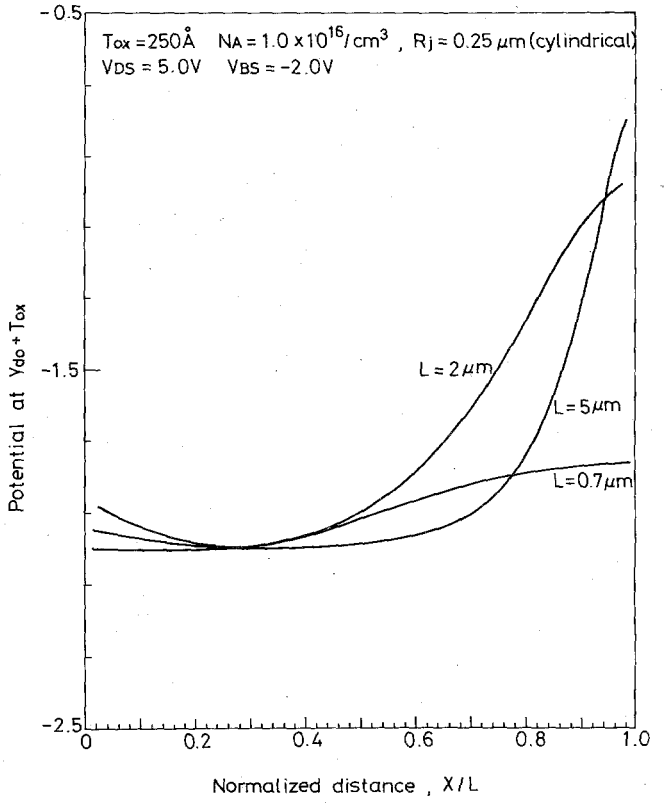

Fig. 5. The calculated potential distributions along the minimum depletion depth for different channel lengths.

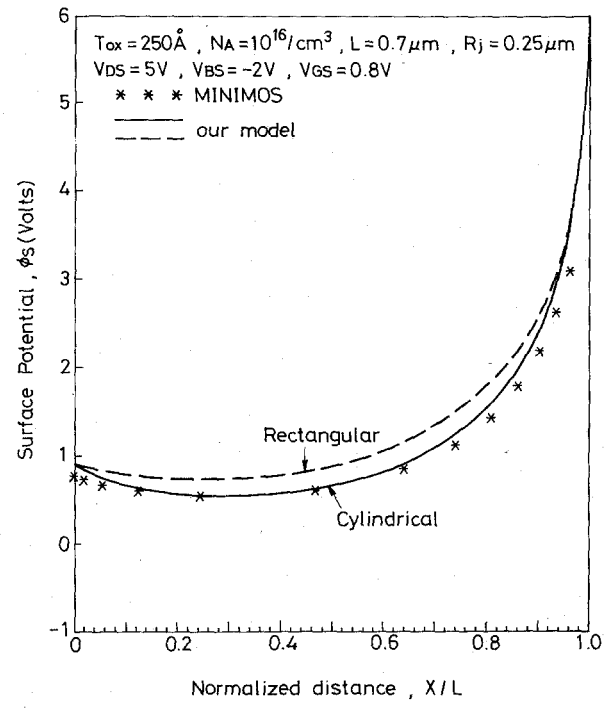

Fig. 6. The calculated potential distributions along the surface channel for different models.

TABLE I
THE INPUT PARAMETERS FOR MINIMOS

Oxide Thickness T_{ox}(Å)	Substrate Doping Concentration N_A(cm^{-3})	Channel Width W(μm)	Source/Drain Junction Depth R_j(μm)
250	1.0×10^{16}	13.5	0.25

Source/Drain Curvature / Source/Drain Profile	Cylindrical
$T_{ox} \le y \le T_{ox} + 0.21$ μm	$1.0 \times 10^{20}/cm^3$
$T_{ox} \le y$	$1.0 \times 10^{20} \cdot \exp\left[-\frac{(y - T_{ox} - 0.21\ \mu m)^2}{2 \cdot (9.32 \times 10^{-7} cm)^2}\right]$

Fig. 3 shows the potential distribution along the surface channel for $L = 0.7$ μm under the specified bias conditions, i.e., $V_{BS} = -2$ V, $V_{DS} = 5$ V, and $V_{GS} = 0.8$ V. The symbol "*" represents the data generated by the two-dimensional numerical analysis—MINIMOS with input parameters illustrated in Table I. The solid curve represents the calculated results using our developed model with the specified source–drain cylindrical junction, and the dash curve represents the results of our developed model with a rectangular-shaped junction and the same junction depth of $R_j = 0.25$ μm. It is clearly seen that comparisons between the solid curve and the MINIMOS's data show quite satisfactory. Moreover, it is obviously shown that the barrier lowering effect for a rectangular-shaped junction is larger than that for a cylindrical junction. This result substantiates our previous statement that the short-channel effects are very sensitive to the specified boundary conditions. Note that the Gaussian profile in the source–drain diffusion islands used in MINIMOS has been chosen to be as abrupt as possible in order to reasonably compare with the abrupt profile used in our model.

III. A Simplified Subthreshold Current Model

In the previous section, the solution of the two-dimensional Poisson's equation has been obtained by neglecting the electron concentration in the conducting channel. This assumption is valid for the MOS device operated in the subthreshold region where the potential distribution is determined primarily by the device geometries, the ionized impurity concentration, and the applied biases. As shown in Fig. 3, the surface potential distribution exhibits a flat-band bending over a certain range along the channel, and the current within this region must be driven by the diffusion component alone. Therefore, the diffusion current in this region can be written as

$$I_{DS} = qD_n\left(\frac{A}{L^*}\right)\left(\frac{n_i^2}{N_A}\right) \cdot \exp\left(\frac{q\Psi^*}{k_BT}\right)\left[1 - \exp\left(-\frac{qV_{DS}}{k_BT}\right)\right] \quad (15)$$

where A is the cross-sectional area of the current flow, D_n is the electron diffusivity, L^* is the effective length of the

region in which the diffusion current dominates, and Ψ^* is the minimum surface potential.

The electron distribution from the surface to the bulk in the subthreshold region can be approximated by the charge sheet model and is expressed by

$$n(x_{\min}, y) = \frac{n_i^2}{N_A} \exp\left(\frac{q\Psi^*}{k_B T}\right) \cdot \exp\left[-\frac{qE_y(y - T_{ox})}{k_B T}\right] \quad (16)$$

where

$$E_y = -\left.\frac{\partial \Psi(x_{\min}, y)}{\partial y}\right|_{y = T_{ox}}.$$

It has been shown that the maximum error produced by the charge sheet model under the weak inversion is only about 4.5 percent [13]. Therefore, the average cross section of the current flow can be approximately written as

$$A = W \frac{\int_{T_{ox}}^{\infty} n(x_{\min}, y)\, dy}{n(x_{\min}, T_{ox})} = W \frac{k_B T}{q|E_y|} \quad (17)$$

where W is the width of the channel.

It should be noted that the effective length L^* in (15) is approximately equal to the channel length (L) for the long-channel MOSFET. However, as the channel length becomes shorter, the derivation between L^* and L becomes much larger. Note that the value of L^* can be self-generated by the calculated surface potential distribution and the criterion is that the region within which the surface potential change is within the value of $\Psi^* + k_B T/q$. In order to check the accuracy of the developed subthreshold current model, the numerical results calculated by MINIMOS [4] are used to compare with our model. The curvature of the source–drain junction is taken to be cylindrical with a radius of 0.25 μm and the doping concentration in the source–drain diffusion island is assumed to be uniform, as listed in Table I. The mobility of electrons (μ_n) is chosen to be 500 ($cm^2/V \cdot s$) as in (15). Comparisons between the results of our model and those computed by MINIMOS are shown in Figs. 7–9 with the specified biases of $V_{DS} = 5$ V, $V_{BS} = 0$ to -2 V. It is clearly seen that the agreement is very satisfactory. It should be noted that no fitting parameters are needed for our developed subthreshold model.

IV. The Threshold Voltage

In general, the threshold voltage deduced from the numerical analysis is often defined as the gate voltage with the drain current equal to a specified value. In order to test the accuracy of the threshold voltage deduced by the subthreshold current model, the numerical results calculated by CADDET [6] with the threshold voltage defined at $I_{DS} = 10^{-8}$ A are used to compare with those calculated by our subthreshold current model. Fig. 10 shows ($V_T - V_{FB}$) versus the effective channel length with the substrate bias as a parameter and under a drain voltage of 5 V. Note that the data points in Fig. 10 are deduced from CADDET and the solid curves are generated by our subthreshold current model. It is clearly seen that the agreement be-

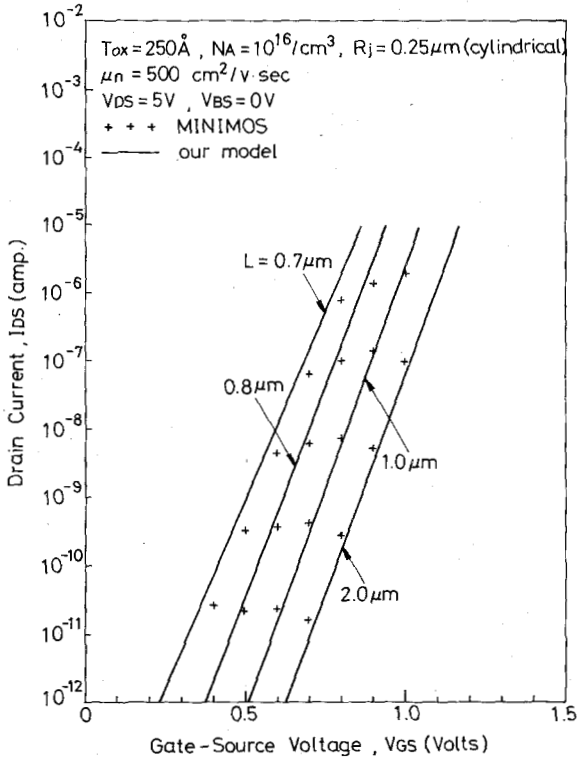

Fig. 7. The calculated subthreshold current versus the applied gate–source voltage for different channel lengths with $V_{BS} = 0$.

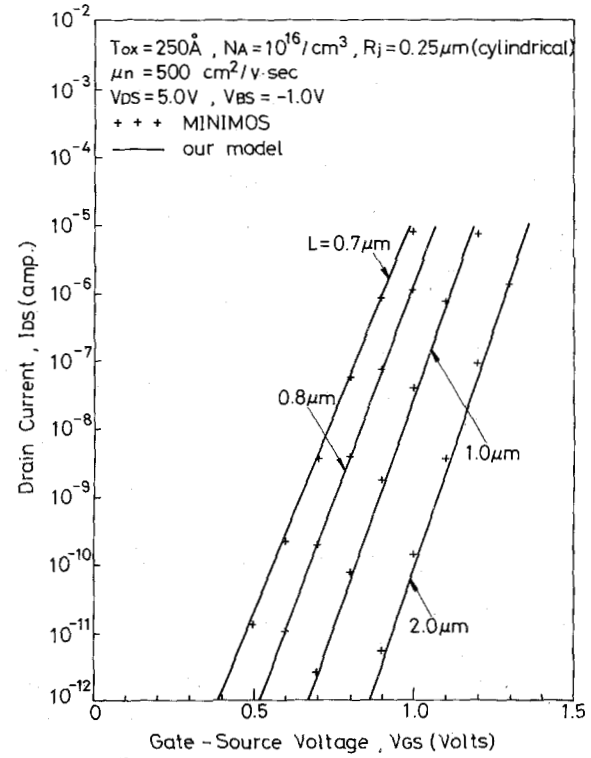

Fig. 8. The calculated subthreshold current versus the applied gate–source voltage for different channel lengths with $V_{BS} = -1$ V.

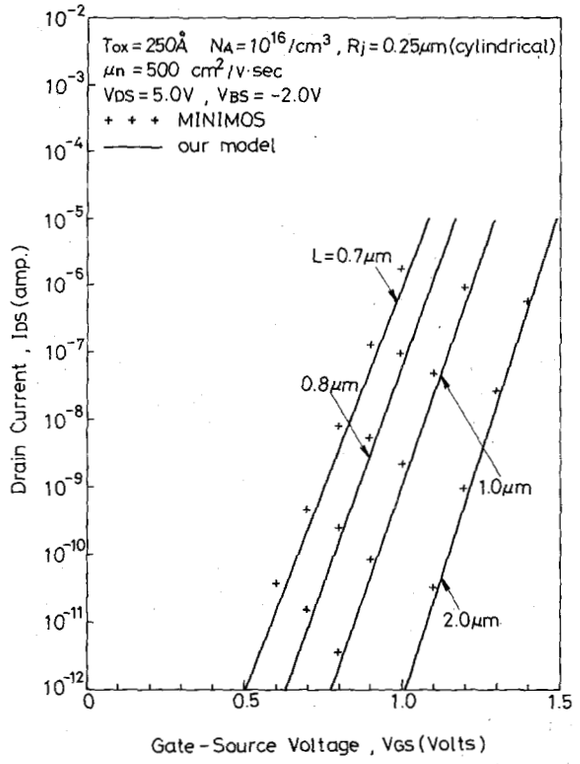

Fig. 9. The calculated subthreshold current versus the applied gate-source voltage for different channel lengths with $V_{BS} = -2$ V.

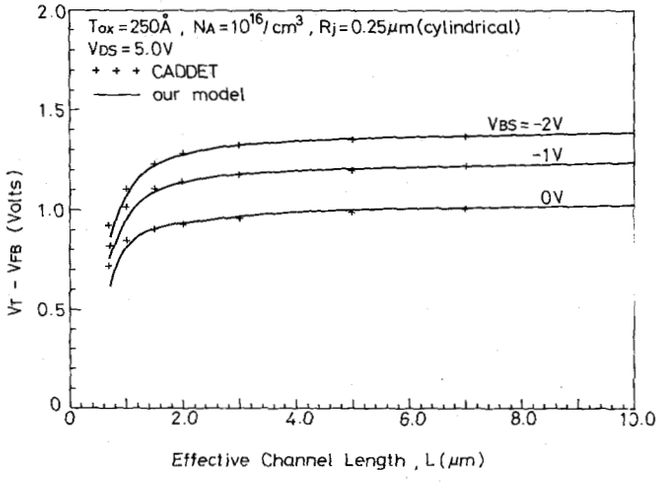

Fig. 10. The calculated $V_T - V_{FB}$ versus the effective channel length for different applied biases.

tween comparisons is very good. Moreover, it is known that the electrical characteristics of short-channel MOSFET's are sensitive to the curvature of the source–drain junction and the profile gradient as well as the junction depth. Therefore, the slight discrepancy for the channel length below 1 μm is mainly due to different doping profiles used in the source–drain islands. Figs. 11 and 12 show ($V_T - V_{FB}$) versus the effective channel length for different oxide thicknesses and substrate doping concentrations, respectively. Comparisons between the experimental data deduced from [6] and the results deduced from our subthreshold current model are shown in Fig. 13.

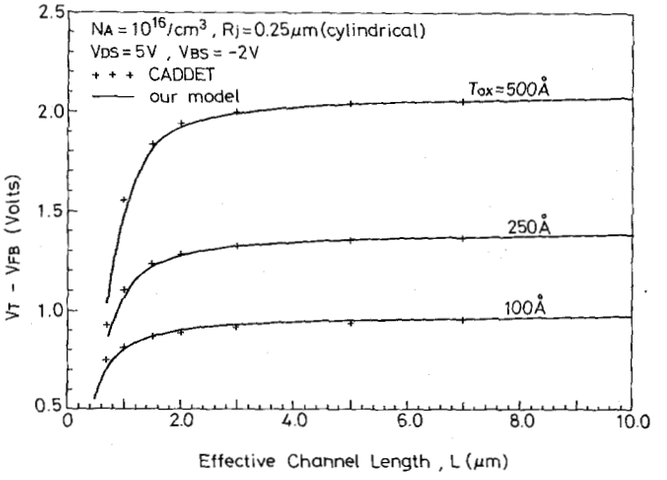

Fig. 11. The calculated $V_T - V_{FB}$ versus the effective channel length for different gate-oxide thicknesses.

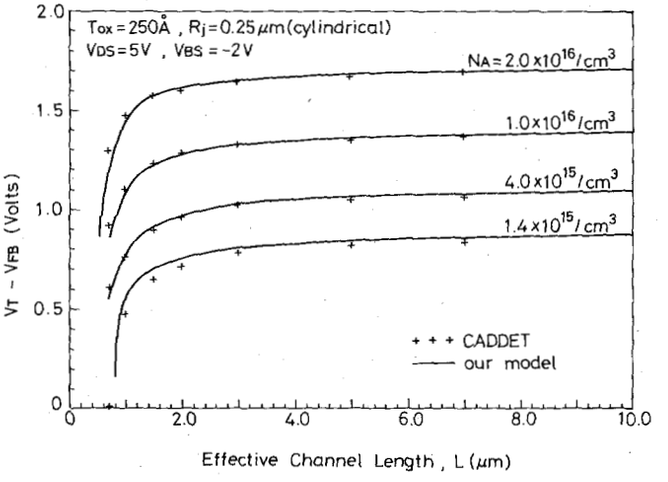

Fig. 12. The calculated $V_T - V_{FB}$ versus the effective channel length for different substrate doping concentrations.

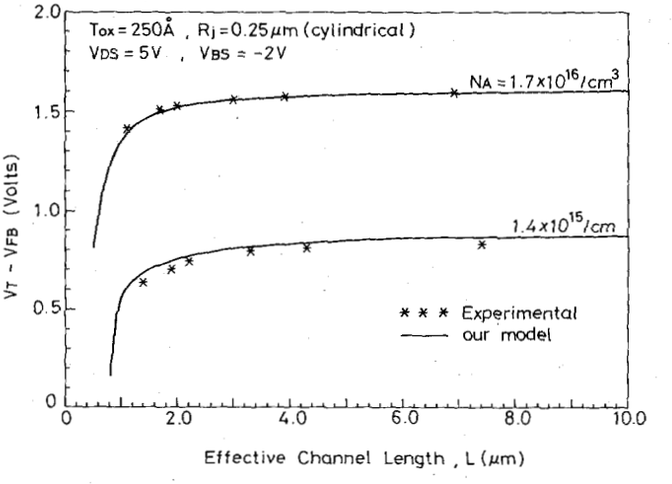

Fig. 13. Comparisons between the calculated $V_T - V_{FB}$ versus the effective channel length and the experimental measurements.

Similarly, good agreement between comparisons has been obtained. Therefore, it is verified that our simplified subthreshold current model is very accurate to deduce the threshold voltage for wide ranges of process parameter variations and applied biases.

V. Conclusion

A two-dimensional model for the potential distribution of short-channel MOSFET's has been developed in this paper. The analytical solution for the two-dimensional Poisson's equation has been obtained by Green's function technique with the appropriate boundary conditions in which the cylindrical curvature with a finite source–drain junction depth is considered. Moreover, no trial solution has been used in our model to calculate the particular solution of the two-dimensional Poisson's equation and the problem of different dielectric permittivities for the oxide and the semiconductor have been solved by the image-charge method. Although the depletion depth is assumed to be independent of the coordinate x, it has been illustrated that the resulting errors are quite negligible. Moreover, it has been demonstrated that the potential distribution of short-channel MOSFET's is very sensitive to the boundary conditions on the source–drain junction. The short-channel effect is overestimated if the source–drain junction is assumed to have a rectangular shape with a finite junction depth. Based on the calculated potential distribution, the subthreshold current and the threshold voltage can be easily calculated. The accuracy of the developed technique has been verified by comparing with the results obtained by two-dimensional numerical analysis and experimental data. Although only the uniform substrate doping is considered in this paper, the developed model can be easily applied to the case with nonuniform substrate doping profile. In future work, the explicit analysis of the subthreshold behavior for short-channel MOSFET's with channel implantation will be developed using the present model.

Appendix
Determination of Image Charge Densities

The values of $\sigma_1(m)$ and $\sigma_2(m)$ can be determined by matching the boundary conditions at the interface $y = T_{ox}$, as illustrated in (9a) and (9b). Expanding the potential $\Psi_0(x, y)$ in terms of the eigenfunction $\sin(k_m x)$, we obtain

$$\Psi_0(x, y) = \sum_{m=\text{odd}}^{\infty} \sin(k_m x) \frac{\rho_A(m)}{\epsilon} \cdot \int_{T_{ox}}^{T_{ox}+Y_{d0}} f(y')\, H(y; y'; k_m)\, dy' + \sum_{m=1}^{\infty} \sin(k_m x)\, B_m(y). \tag{A1}$$

For the uniform doping case, $f(y') = 1$ and $B_m(y)$ in (A1) can be expressed as

$$B_m(y) = \frac{\sinh k_m(b-y)}{\sinh(k_m b)} \cdot \frac{4V'_{GS}}{m\pi} + \frac{\sinh(k_m y)}{\sinh(k_m b)} \cdot \frac{4V_{BS}}{m\pi} + \frac{2k_m}{L} \int_0^b \phi(0, y')\, H(y; y'; k_m)\, dy' + (-1)^{m+1} \frac{2k_m}{L} \int_0^b \phi(L, y')\, H(y; y'; k_m)\, dy'. \tag{A2}$$

Substituting the above equations into (9a) and (9b), we obtain

$$\frac{\sigma_1(m)}{\epsilon_{si}} - \frac{\sigma_2(m)}{\epsilon_{ox}} = \frac{1-(-1)^m}{2}(1/\epsilon_{ox} - 1/\epsilon_{si}) \cdot \rho_A(m) \frac{\cosh k_m(b - T_{ox}) - \cosh k_m(b - T_{ox} - Y_{d0})}{k_m \sinh k_m(b - T_{ox})} \tag{A3}$$

and

$$\sigma_1(m) \frac{\cosh k_m(b - T_{ox}) \sinh(k_m T_{ox})}{\sinh(k_m b)} + \sigma_2(m) \frac{\cosh(k_m T_{ox}) \sinh k_m(b - T_{ox})}{\sinh(k_m b)} = (\epsilon_{si} - \epsilon_{ox}) \frac{\partial}{\partial y} B_m(y)\Big|_{y = T_{ox}}. \tag{A4}$$

Therefore, the values of $\sigma_1(m)$ and $\sigma_2(m)$ can be obtained by the above equations.

Acknowledgment

The authors would like to express their sincere thanks to Dr. C. T. Shih and Dr. C. C. Chang for helpful discussions and support.

References

[1] Y. El-mansy, "MOS device and technology constraints in VLSI," *IEEE Trans. Electron Devices*, vol. ED-29, pp. 567–573, Apr. 1982.
[2] R. R. Troutman, "VLSI limitation from drain-induced barrier lowering," *IEEE Trans. Electron Devices*, vol. ED-26, no. 4, pp. 461–468, Apr. 1979.
[3] B. Eitan and D. Frohman-Bentchkowsky, "Surface conduction in short-channel MOS device as a limitation to VLSI scaling," *IEEE Trans. Electron Devices*, vol. ED-29, pp. 254–264, Feb. 1982.
[4] S. Selberherr, A. Schütz, and H. W. Pötzl, "MINIMOS—A two-dimensional MOS transistor analyzer," *IEEE Trans. Electron Devices*, vol. ED-27, pp. 1540–1549, Aug. 1980.
[5] C. L. Wilson, P. Roitman, and J. L. Blue, "High-accuracy physical modeling of submicronmeter MOSFET's," *IEEE Trans. Electron Devices*, vol. ED-32, pp. 1246–1258, July 1985.
[6] T. Toyabe and S. Asai, "Analytical models of threshold voltage and breakdown voltage of short-channel MOSFET's derived from two-dimensional analysis," *IEEE Trans. Electron Devices*, vol. ED-26, pp. 453–461, Apr. 1979.
[7] C. Y. Wu and S. Y. Yang, "An analytic and accurate model for the

threshold voltage of short channel MOSFETs in VLSI," *Solid-State Electron.*, vol. 27, pp. 651–658, July 1984.
[8] K. N. Ratnakumar and J. D. Meindl, "Short-channel MOST threshold voltage model," *IEEE J. Solid-State Circuits*, vol. SC-17, pp. 937–947, Oct. 1982.
[9] D. R. Poole and D. L. Kwong, "Two-dimensional analytical modeling of threshold voltage of short-channel MOSFET's," *IEEE Electron Device Lett.*, vol. EDL-5, pp. 443–446, Nov. 1984.
[10] J. R. Pfiester, J. D. Shott, and J. D. Meindl, "Performance limits of CMOS ULSI," *IEEE Trans. Electron Devices*, vol. ED-32, pp. 323–343, Feb. 1985.
[11] J. D. Jackson, *Classical Electrodynamics*. New York: Wiley, 1975.
[12] C. R. Viswanathan, B. C. Burkey, G. Lubberts, and T. J. Tredwell, "Threshold voltage in short-channel MOS devices," *IEEE Trans. Electron Devices*, vol. ED-32, pp. 932–940, May 1985.
[13] J. R. Brews, "A charge-sheet model of the MOSFET," *Solid-State Electron.*, vol. 21, pp. 345–355, Feb. 1978.

*

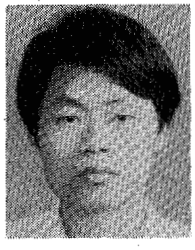

Pole-Shang Lin (S'85) was born in Taiwan, Republic of China, on May 29, 1960. He received the B.S. degree in electrical engineering from National Chiao-Tung University, Republic of China, in 1982. In 1984, he entered the Institute of Electronics, National Chiao-Tung University, for graduate study and, in 1985, became a candidate for the Ph.D. degree.

During 1982–1984, he joined the military service and taught electronics at the Chinese Army Communication School. His present research interests include the analytic modeling of small-geometry MOS devices in VLSI and thin-film transistors for flat-panel display.

Mr. Lin is a member of Phi Tau Phi.

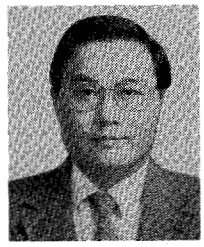

Ching-Yuan Wu (S'69–M'72) was born in Taiwan, Republic of China, on March 18, 1946. He received the B.S. degree from the Department of Electrical Engineering, National Taiwan University, Taiwan, Republic of China, in 1968, and the M.S. and Ph.D. degrees from the State University of New York (SUNY) at Stony Brook, in 1970 and 1972, respectively.

During the 1968–1969 academic year, he served in the Chinese Air Forces as a Second Lieutenant. During the 1972–1973 academic year, he was appointed as a Lecturer at the Department of Electrical Sciences, SUNY, Stony Brook. During the 1973–1975 academic years, he was a Visiting Associate Professor at National Chiao-Tung University (NCTU), Taiwan, Republic of China. In 1976, he became a Full Professor in the Department of Electronics and the Institute of Electronics, NCTU. During 1974–1980, he had been the Director of Engineering Laboratories and Semiconductor Research Center, NCTU. He was a Principal Investigator of the National Electronics Mass Plan—Semiconductor Devices and Integrated-Circuit Technologies, during 1976–1979. He was the Director of the Institute of Electronics, NCTU, during 1978–1984. Since 1984, he has been the Dean, College of Engineering, NCTU. He has also been the Research Consultant of the Electronics Research and Service Organization (ERSO), ITRI, and the Academic Advisory Member of the Ministry of Education, Republic of China. He has been the Coordinator of the Microelectronics Research and Development Committee, National Science Council, Republic of China. His research activities have been in semiconductor device physics and modeling, integrated-circuit design, and technologies. His present research interests focus on small geometry devices in VLSI, CMOS latchup, new devices, and technologies. He has published over 120 papers in the semiconductor field.

Dr. Wu is a member of Phi Tau Phi and an Editor of the Journal of the Chinese Institute of Engineers in Electrical Engineering. He received the Academic Research Award in Engineering from the Ministry of Education, in 1979, and the Outstanding Scholar award from the Chinese Educational and Cultural Foundation, Republic of China, in 1985, and has received the Outstanding Research Professor Fellowship from the Ministry of Education and the National Science Council, Republic of China, during 1982–1986.